INTERNATIONAL JOURNAL FOR NUMERICAL AND ANALYTICAL METHODS IN GEOMECHANICS, VOL. 9, 525–539 (1985)

TORSIONAL STIFFNESS OF NON-UNIFORM AND HOLLOW RIGID PIERS EMBEDDED IN ISOTROPIC ELASTIC MEDIA

R. K. N. D. RAJAPAKSE* AND A. P. S. SELVADURAI†

Department of Civil Engineering, Carleton University, Ottawa, Ontario, Canada K1S 5B6

SUMMARY

This paper examines the torsional response of a rigid pier type foundation, with a non-uniform or hollow cross-section which is embedded in bonded contact with a layered elastic half space. The tractions which act at the axisymmetric boundary surface between the pier and the surrounding elastic medium are represented by discretized regions of uniform traction. The compatibility of deformation at the boundary is used to determine the interface stress distribution. The torque–rotation response for the rigid pier foundation is obtained for different choices of the pier geometry and shear modulus mismatch between the layer and the underlying half space.

INTRODUCTION

Rigid piers are used quite extensively as structural foundations for isolated structures such as power transmission towers, housing of solar cell arrays and anchors for floating structures. These structural foundations are usually cylindrical in shape and on occasions the foundations can be constructed with a non-uniform or tapered section (Figure 1). Such non-uniformity can exist naturally as in the case of timber piles or it can be purposely introduced to enhance the stiffness of the structural foundation. Another common type of foundation is the hollow pier or caisson-type foundation (Figure 1) which is extensively used to support offshore structures. These pier type structures can be subjected to significant torsional loads as a result of non-uniform tension in the transmission lines, created by wind or ice action. In the case of offshore structures significant torsional loads can be induced by wave or wind action and also due to accidental collisions with ice floes or icebergs. The assessment of the torsional stiffness of these structural foundations is therefore important to the static and dynamic analysis of structure–foundation systems.

The analytical study of torsion of cylindrical inclusions embedded in elastic media has received some attention. Poulos[1], analysed the torsion of embedded uniform piles by employing a discretization scheme. An exact analytical solution was presented by Luco[2] for a rigid uniform cylinder embedded in a layered elastic half space. Integral representations were used to reduce the problem to the solution of two integral equations. These in turn were solved by using an appropriate numerical scheme. Recently Karasudhi, Rajapakse and Hwang[3] solved the problem of torsion of an elastic bar partially embedded in a layered elastic half space. The method employed was similar to that presented by Muki and Sternberg[4]. However a different compatibility condition was used to incorporate the stress singularity at the base of the bar and the resulting Fredholm

* Postdoctoral Research Fellow
† Professor and Chairman

0363-9061/85/060525-15$01.50

Received 23 February 1984
Revised 20 June 1984

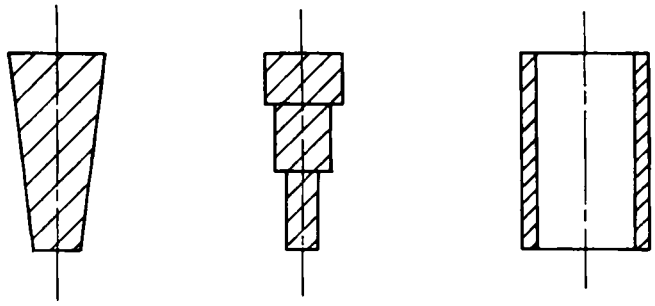

Figure 1. Rigid pier foundations

integral equation was solved by employing an appropriate numerical method. In this investigation it was observed that, except for very short piers, the stress singularity at the base of the pier has a negligible effect on the computed torque–twist relationship for the embedded pier. In the above studies,[1-3] the geometry of the bar is restricted to the simplified uniform cylindrical shape. To the authors' knowledge the problem related to the estimation of the torsional stiffness of a non-uniform rigid pier or a hollow cylindrical pier embedded in a layered half space has not been considered in the literature.

This paper focuses on the evaluation of the torsional stiffness of non-uniform and hollow rigid piers embedded in bonded contact with an isotropic layered elastic half space and subjected to a torque at the free end (Figure 2). The torsional loading of the axisymmetric pier imposes a state of rotational symmetry in the stress and deformation fields. Therefore analysis of the torsion problem is performed by employing a fundamental solution related to a concentrated circular torsional ring load acting at the interior of an isotropic elastic half space. The axisymmetric boundary surface between the pier and the surrounding elastic medium is discretized by regions of uniform traction. The compatibility of deformation between the rigid pier and the elastic medium is used to determine the interface stress distribution. The torque–rotation response for the pier foundation is

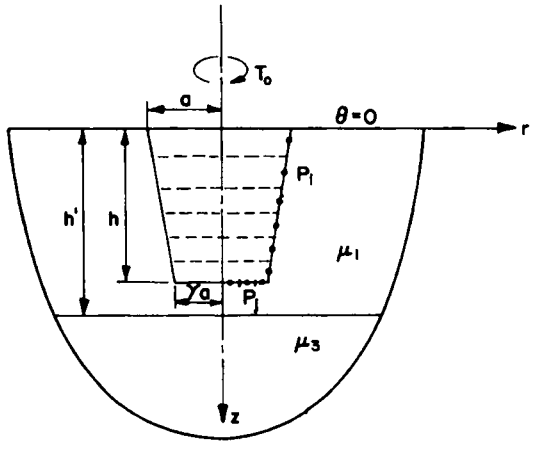

Figure 2. Discretization of a rigid pier

obtained for different choices of the pier geometry. The numerical results are also compared with existing solutions[2,3] for uniform cylindrical piers embedded in isotropic elastic media.

FUNDAMENTAL SOLUTION

Figure 3 shows the layered elastic half space, and the cylindrical polar co-ordinate system (r, θ, z) is chosen such that the z-axis is normal to the free surface of the half space region. The problems under consideration posses a state of symmetry about the z-axis and the functions involved are independent of the azimuthal co-ordinate θ. Owing to the state of symmetry imposed by axisymmetric torsion, the displacements u and w, in the r and z directions, respectively, vanish; and in the absence of body forces, the non-zero displacement component v in the θ direction is governed by the displacement equation of equilibrium

$$\frac{\partial^2 v}{\partial r^2} - \frac{v}{r^2} + \frac{1}{r}\frac{\partial v}{\partial r} + \frac{\partial^2 v}{\partial z^2} = 0 \tag{1}$$

The non-zero stress components $\sigma_{r\theta}$ and $\sigma_{\theta z}$ referred to the cylindrical polar co-ordinate system can be expressed as

$$\sigma_{\theta z} = \mu \frac{\partial v}{\partial z} \qquad \sigma_{r\theta} = \mu\left(\frac{\partial v}{\partial r} - \frac{v}{r}\right) \tag{2}$$

where μ is the linear elastic shear modulus of the medium.

The general solution of (1) is obtained by employing a Hankel transform development with respect to the radial co-ordinate.[5] Following Sneddon[6] it can be shown that generalized solution for the displacement v can be expressed in the form

$$v(r, z) = \int_0^\infty (A e^{-\xi z} + B e^{\xi z}) J_1(\xi r)\, d\xi \tag{3}$$

Where J_1 is the Bessel function of the first kind of the first order, and $A(\xi)$ and $B(\xi)$ are arbitrary functions which should be determined by invoking appropriate boundary and continuity conditions. At this stage it is convenient to non-dimensionalize the problem by defining a which denotes the radius of the embedded rigid pier at $z = 0$, as a unit length.

In order to develop the solutions corresponding to torsional ring loads of finite extent it is necessary to derive the displacements due to a concentrated circular ring torque applied at the

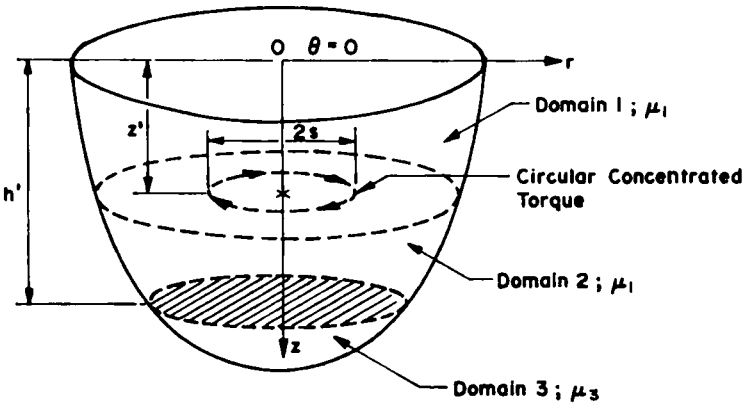

Figure 3. Circular concentrated torque in the interior of layered half space

interior of a layered half space region (see, for instance, Figure 3). By defining a fictitious plane at $z = z'$, we can reduce the problem to one which has three domains (see Figure 3). The superscript or subscript $i(i = 1, 2, 3)$ is used to identify the quantities associated with each domain. The displacement field in each domain has the general form given by equation (3) consisting of two functions $A_i(\xi)$ and $B_i(\xi)$. In domain 3 however, to ensure regularity of displacements and stresses derived from equation (3) the term $B_3(\xi) \equiv 0$. The remaining five functions $[A_i(\xi)\ (i = 1, 2, 3), B_i(\xi)(i = 1, 2)]$ are determined from the following boundary and continuity conditions

$$\sigma_{\theta z}^{(1)}(r, 0) = 0 \tag{4a}$$

$$v^{(1)}(r, z') = v^{(2)}(r, z') \tag{4b}$$

$$\sigma_{\theta z}^{(1)}(r, z') - \sigma_{\theta z}^{(2)}(r, z') = \delta(r - s) = \int_0^\infty s\xi J_1(\xi s) J_1(\xi r)\, d\xi \tag{4c}$$

$$v^{(2)}(r, h') = v^{(3)}(r, h') \tag{4d}$$

$$\sigma_{\theta z}^{(2)}(r, h') = \sigma_{\theta z}^{(3)}(r, h') \tag{4e}$$

The above conditions are valid for the case where $z' < h'$ and the corresponding expressions for the case $z' > h'$ could be obtained in a similar fashion. The solution of the resulting system of simultaneous equations leads to the following expressions for the displacement fields in each domain. For $z' \leqslant h'$

$$\left.\begin{matrix} v^{(1)}(r, z) \\ v^{(2)}(r, z) \end{matrix}\right\} = \frac{1}{2\mu_1(1+\alpha)} \int_0^\infty \frac{sJ_1(\xi s) J_1(\xi r)}{H(\xi h')} [(1+\alpha)(e^{-\xi(z+z')} + e^{-\xi|z-z'|}) + (1-\alpha)(e^{-\xi(2h'-z-z')} + e^{-\xi(2h'-|z-z'|)})]\, d\xi, \quad (0 \leqslant z \leqslant h') \tag{5a}$$

$$v^{(3)}(r, z) = \frac{1}{\mu_1(1+\alpha)} \int_0^\infty \frac{sJ_1(\xi s) J_1(\xi r)}{H(\xi h')} [e^{-\xi(z+z')} + e^{-\xi(z-z')}]\, d\xi, \quad (h' \leqslant z < \infty) \tag{5b}$$

For $z' \geqslant h'$

$$v^{(1)}(r, z) = \frac{1}{\mu_1(1+\alpha)} \int_0^\infty \frac{sJ_1(\xi s) J_1(\xi r)}{H(\xi h')} [e^{-\xi(z+z')} + e^{-\xi(z'-z)}]\, d\xi, \quad (0 \leqslant z \leqslant h') \tag{6a}$$

$$\left.\begin{matrix} v^{(2)}(r, z) \\ v^{(3)}(r, z) \end{matrix}\right\} = \frac{1}{2\alpha\mu_1(1+\alpha)} \int_0^\infty \frac{sJ_1(\xi s) J_1(\xi r)}{H(\xi h')} [(1+\alpha)(e^{-\xi(z+z')} + e^{-\xi|z-z'|}) - (1-\alpha)(e^{-\xi(z+z'-2h')} + e^{-\xi(2h'+|z-z'|)})]\, d\xi, \quad (h' \leqslant z < \infty) \tag{6b}$$

where

$$H(\xi h') = [(1+\alpha) - (1-\alpha)e^{-2\xi h'}]/(1+\alpha)$$

and

$$\alpha = \mu_3/\mu_1$$

AXISYMMETRIC TORSION OF A RIGID PIER

We consider the problem of non-uniform rigid pier embedded in a layered elastic half space (Figure 2). It is assumed that the pier is perfectly bonded to the surrounding layered elastic half

space. In order to evaluate the torsional stiffness of the pier we discretize the axisymmetric boundary surface between the pier and elastic medium by regions of uniform traction. It may be observed that the bounding surface of any rigid pier can be discretized by using a combination of the three fundamental ring elements shown in Figure 4. These are identified as vertical elements (VE), base or horizontal elements (BE) and inclined elements (IE). It is assumed that the unknown traction is uniform across the element for VE and IE whereas for BE the traction varies linearly, as shown in Figure 4. The displacement at point $P_i(r_1, z_i)$ due to element j is denoted by f_{ij} and the unknown traction acting on the jth element is denoted by T_j. If we denote the rotation of the pier by ϕ_0 then the compatibility condition gives

$$\sum_{j=1}^{N} T_j f_{ij} = \phi_0 r_i, \quad i = 1, 2, \ldots, N \tag{7}$$

where N is the number of elements used to discretize the boundary surface. Equation (7) can be solved for $T_j (j = 1, 2, \ldots, N)$ by specifying $\phi_0 = 1$, and expressions for f_{ij} could be derived from the fundamental solutions presented in equations (5) and (6). Before deriving the expressions for f_{ij} it is necessary to express the common denominator $H(\xi h')$ appearing in equations (5) and (6) in a convenient exponential form to avoid lengthy numerical integration of the infinite integrals. By following the scheme presented by Chan *et al.*[7] the denominator $H(\xi h')$ could be approximated for various values of α and h' as

$$\frac{1}{H(\xi h')} = \sum_{m=1}^{M} a_m e^{-2(m-1)h'} \tag{8}$$

The values of a_m can be determined from the integral least squares method. For most practical purposes it is found[3,7] that very accurate solutions can be obtained by specifying the value of M to be equal to five. Employing the representation (8) and performing the appropriate integrations across the thickness of the jth element, the following expressions are derived for f_{ij}.

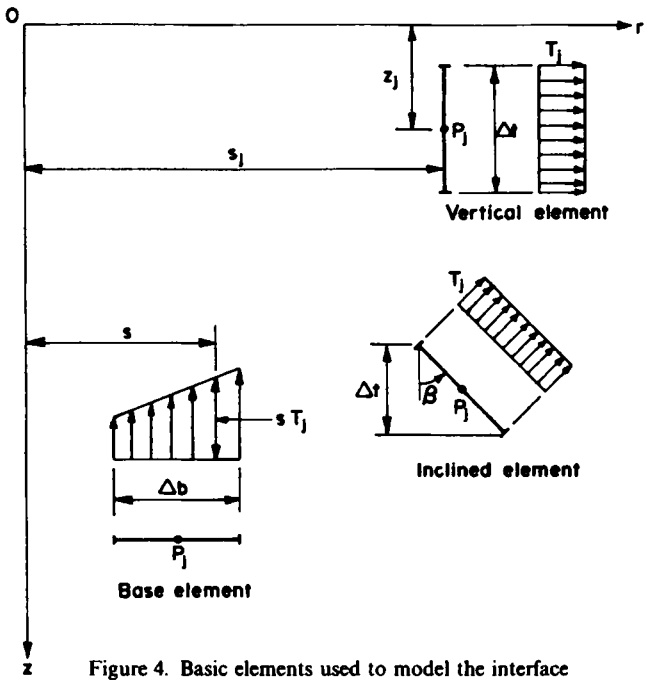

Figure 4. Basic elements used to model the interface

For a vertical element, $(z_j + \Delta t/2) \leqslant h'$

$$f_{ij} = \frac{1}{2\mu_1(1+\alpha)} \sum_{m=1}^{5} a_m [-(1+\alpha)\phi_m(1,1;-1) + (1-\alpha)\psi_m(1,1;-1)]_{z'=z_j^1}^{z'=z_j^2} \quad (z_i \leqslant z_j^1) \tag{9a}$$

$$f_{ij} = \frac{1}{2\mu_1(1+\alpha)} \sum_{m=1}^{5} a_m [-(1+\alpha)\bar{\phi}_m(1,1;-1) + (1-\alpha)\bar{\psi}_m(1,1;-1)]_{z'=z_j^1}^{z'=z_j^2} \quad (z_i \geqslant z_j^2) \tag{9b}$$

$$f_{ij} = \frac{1}{2\mu_1(1+\alpha)} \sum_{m=1}^{5} a_m \{[-(1+\alpha)\bar{\phi}_m(1,1;-1) + (1-\alpha)\bar{\psi}_m(1,1;-1)]_{z'=z_j^1}^{z'=z_i} + [-(1+\alpha)\phi_m(1,1;-1) + (1-\alpha)\psi_m(1,1;-1)]_{z'=z_i}^{z'=z_j^2}\} \quad (z_j^1 < z_i < z_j^2) \tag{9c}$$

$$f_{ij} = \frac{1}{\mu_1(1+\alpha)} \sum_{m=1}^{5} a_m [\phi_m(1,1;-1)]_{z'=z_j^1}^{z'=z_j^2} \quad (z_i \geqslant h') \tag{9d}$$

For a vertical element, $(z_j - \Delta t/2) \geqslant h'$

$$f_{ij} = \frac{1}{\mu_1(1+\alpha)} \sum_{m=1}^{5} a_m [\phi_m(1,1;-1)]_{z'=z_j^1}^{z'=z_j^2} \quad (z_i \leqslant h') \tag{10a}$$

$$f_{ij} = \frac{1}{2\alpha\mu_1(1+\alpha)} \sum_{m=1}^{5} a_m [-(1+\alpha)\phi_m(1,1;-1) + (1-\alpha)\psi_m(1,1;-1)]_{z'=z_j^1}^{z'=z_j^2} \quad (h' \leqslant z_1 \leqslant z_j^1) \tag{10b}$$

$$f_{ij} = \frac{1}{2\alpha\mu_1(1+\alpha)} \sum_{m=1}^{5} a_m [-(1+\alpha)\bar{\phi}_m(1,1;-1) + (1-\alpha)\bar{\psi}_m(1,1;-1)]_{z'=z_j^1}^{z'=z_j^2} \quad (h' \leqslant z_j^2 \leqslant z_i) \tag{10c}$$

$$f_{ij} = \frac{1}{2\alpha\mu_1(1+\alpha)} \sum_{m=1}^{5} a_m \{[-(1+\alpha)\bar{\phi}_m(1,1;-1) + (1-\alpha)\bar{\psi}_m(1,1;-1)]_{z'=z_j^1}^{z'=z_i} + [-(1+\alpha)\phi_m(1,1;-1) + (1-\alpha)\psi_m(1,1;-1)]_{z'=z_i}^{z'=z_j^2}\} \quad (z_j^1 < z_i < z_j^2) \tag{10d}$$

For a base element, $z_j \leqslant h'$

$$f_{ij} = \frac{1}{2\mu_1(1+\alpha)} \sum_{m=1}^{5} a_m [(1+\alpha)\phi_m(1,2;-1) + (1-\alpha)\psi_m(1,2;-1)]_{s=s_j^1}^{s=s_j^2} \quad (z_i \leqslant h') \tag{11a}$$

$$f_{ij} = \frac{1}{\mu_1(1+\alpha)} \sum_{m=1}^{5} a_m [\phi_m(1,2;-1)]_{s=s_j^1}^{s=s_j^2} \quad (z_i \geqslant h') \tag{11b}$$

For a base element, $z_j \geqslant h'$

$$f_{ij} = \frac{1}{\mu_1(1+\alpha)} \sum_{m=1}^{5} a_m [\phi_m(1,2;-1)]_{s=s_j^1}^{s=s_j^2} \quad (z_i \leqslant h') \tag{12a}$$

$$f_{ij} = \frac{1}{2\alpha\mu_1(1+\alpha)} \sum_{m=1}^{5} a_m [(1+\alpha)\phi_m(1,2;-1) + (1-\alpha)\psi_m(1,2;-1)]_{s=s_j^1}^{s=s_j^2} \quad (z_i \geqslant h') \tag{12b}$$

For an inclined element, $(z_j + \Delta t/2) \leqslant h'$

$$f_{ij} = \frac{1}{2\mu_1(1+\alpha)} \sum_{m=1}^{5} a_m \left\{ \int_{z_j^1}^{z_j^2} [(1+\alpha)\phi_m(1,1;0) + (1-\alpha)\psi_m(1,1;0)] \frac{dz'}{\cos\beta} \right\} \quad (z_i \leqslant h') \tag{13a}$$

$$f_{ij} = \frac{1}{\mu_1(1+\alpha)} \sum_{m=1}^{5} a_m \left[\int_{z_j^1}^{z_j^2} \phi_m(1,1;0) \frac{dz'}{\cos\beta} \right] \quad (z_i \geqslant h') \tag{13b}$$

For an inclined element, $(z_j - \Delta t/2) \geqslant h'$

$$f_{ij} = \frac{1}{\mu_1(1+\alpha)} \sum_{m=1}^{5} a_m \left[\int_{z_j^1}^{z_j^2} \phi_m(1,1;0) \frac{dz'}{\cos\beta} \right] \quad (z_i \geqslant h') \tag{14a}$$

$$f_{ij} = \frac{1}{2\alpha\mu_1(1+\alpha)} \sum_{m=1}^{5} a_m \left\{ \int_{z_j^1}^{z_j^2} [(1+\alpha)\phi_m(1,1;0) - (1-\alpha)\psi_m(1,1;0)] \frac{dz'}{\cos\beta} \right\} \quad (z_i \geqslant h') \tag{14b}$$

where
$$\phi_m(p,q;\lambda) = s^q[I_{1m}(p,q;\lambda) + I_{2m}(p,q;\lambda)] \tag{15a}$$

$$\bar{\phi}_m(p,q;\lambda) = s^q[I_{1m}(p,q;\lambda) - I_{2m}(p,q;\lambda)] \tag{15b}$$

$$\psi_m(p,q;\lambda) = s^q[I_{3m}(p,q;\lambda) + I_{4m}(p,q;\lambda)] \tag{15c}$$

$$\bar{\psi}_m(p,q;\lambda) = s^q[I_{3m}(p,q;\lambda) - I_{4m}(p,q;\lambda)] \tag{15d}$$

and

$$I_{1m}(p,q;\lambda) = \int_0^\infty J_p(\xi r_i) J_q(\xi s) \xi^\lambda e^{-\xi[z_i + z' + 2(m-1)h']} d\xi \tag{16a}$$

$$I_{2m}(p,q;\lambda) = \int_0^\infty J_p(\xi r_i) J_q(\xi s) \xi^\lambda e^{-\xi[|z_i + z'| + 2(m-1)h']} d\xi \tag{16b}$$

$$I_{3m}(p,q;\lambda) = \int_0^\infty J_p(\xi r_i) J_q(\xi s) \xi^\lambda e^{-\xi[|2h' - z_i - z'| + 2(m-1)h']} d\xi \tag{16c}$$

$$I_{4m}(p,q;\lambda) = \int_0^\infty J_p(\xi r_i) J_q(\xi s) \xi^\lambda e^{-\xi[2h' - |z_i - z'| + 2(m-1)h']} d\xi \tag{16d}$$

$$[f(t)]_{t=t_2}^{t=t_1} = f(t_1) - f(t_2) \tag{17a}$$

$$z_j^1 = z_j - \Delta t/2; \quad z_j^2 = z_j + \Delta t/2 \tag{17b}$$

$$s_j^1 = s_j - \Delta b/2; \quad s_j^2 = s_j + \Delta b/2 \tag{17c}$$

In the case of vertical and base elements it is possible to perform analytical integration across the thickness of the element in deriving the expressions for f_{ij} from the fundamental solutions presented in equations (5) and (6). However, as can be seen from equations (13) and (14) for an inclined element it is impossible to perform analytical integration over the width of the element. Thus a numerical integration scheme should be used in evaluating f_{ij} for the inclined element and the details are presented in the ensuing section.

NUMERICAL SOLUTION SCHEME

The numerical solution of the flexibility equation involves the computation of f_{ij} at each mesh point on the boundary surface. The expressions of f_{ij} presented in equations (9)–(14) involve integrals of the Lipschitz–Hankel type.[8] Eason *et al.*[9] examined these integrals and expressed them in terms of functions tabulated by Heuman.[10] The functions tabulated by Heuman are symbolically represented by F_0, E_0, and Λ_0. These functions are directly related to complete elliptic integrals of the first, second and third kinds.[10, 11] In evaluating the integrals $I_{1m}, \ldots, I_{4m}$ appearing in the equations we use the expressions presented by Eason *et al.* for $I(1,1;-1)$, $I(1,0;-1)$ and $I(1,1;0)$, and the following recurrence relationships to evaluate $I(1,2;-1)$:

$$s[I(1,2;-1) + I(1,0;-1)] = 2I(1,1;-2) \tag{18a}$$

$$I(1,1;-2) = [rI(0,1;-1) + sI(1,0;-1) - cI(1,1;-1)]/3 \tag{18b}$$

where

$$I(p,q;\lambda) = \int_0^\infty J_p(\xi r) J_q(\xi s) \xi^\lambda e^{-c\xi} d\xi \tag{18c}$$

The numerical values of F_0 and E_0 are computed by using the series expansion presented by Abramowitz and Stegun.[11] Since there are no such general expansions available for Λ_0 we need to perform numerical integrations to evaluate Λ_0. Thus in this study Λ_0 is evaluated by using the Gauss quadrature formula with thirty two quadrature points[11] to ensure accurate estimation of Λ_0. It should also be mentioned here that the Lipschitz–Hankel type integrals appearing in the integrands of equations (13) and (14) could be computed by using E_0 and F_0 only; this provides an economical technique for the numerical integration of the integrals. In evaluating f_{ij} given by equations (13) and (14) it is sufficient to use an extended Simpson's rule[11] integration with ten subdivisions.

Based on the above solution scheme and the associated numerical procedures the authors have developed a computer code to evaluate the stiffness of rigid piers. The inputs to the program are the shear moduli of the elastic media, co-ordinates of node points, thickness of the top layer and the values of a_m appearing in equation (8). The procedures outlined previously may convey the impression that the solution scheme involves considerable numerical effort, especially when considering the number of Lipschitz–Hankel type integrals which need to be evaluated for the computation of f_{ij} for a given pier geometry and elastic properties of the layered media. A careful inspection of expressions for f_{ij} reveals the fact that the values of ϕ_m, $\bar{\phi}_m$, ψ_m and $\bar{\psi}_m$ are independent of elastic moduli of the media. Thus for a given pier geometry we can compute ϕ_m, $\bar{\phi}_m$, ψ_m, $\bar{\psi}_m$ and store the information in the computer memory. Subsequently we can compute f_{ij} for any value of α by simple multiplication of the functions by a_m according to the expression for f_{ij} presented in equations (9)–(14). In this approach we need to compute the Lipschitz–Hankel integrals only once for a given pier geometry, and compute f_{ij} corresponding to as many values of $\alpha = \mu_3/\mu_1$ as desired. This scheme would result in a considerable reduction in computer time and should be followed in similar problems involving torsional loading of a layered half space region.

DISCUSSION OF RESULTS AND CONCLUSIONS

Frequently in geotechnical applications the length of the rigid pier may be equal to the thickness of the top layer. This is usually dictated by the soil conditions at a site. The numerical results

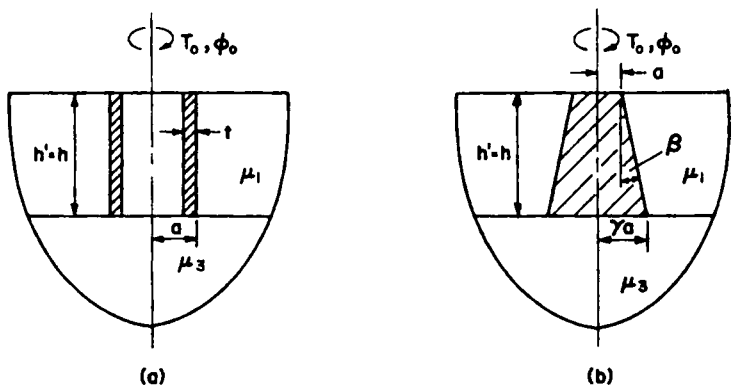

Figure 5. Problems considered in parametric study

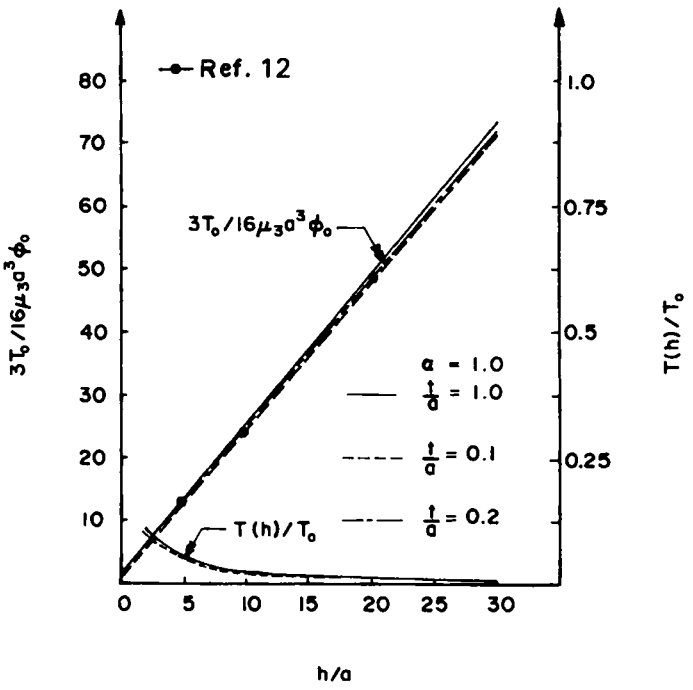

Figure 6. Variation of torsional stiffness and proportion of torque transfer at base for a hollow pier ($\alpha = 1{\cdot}0$)

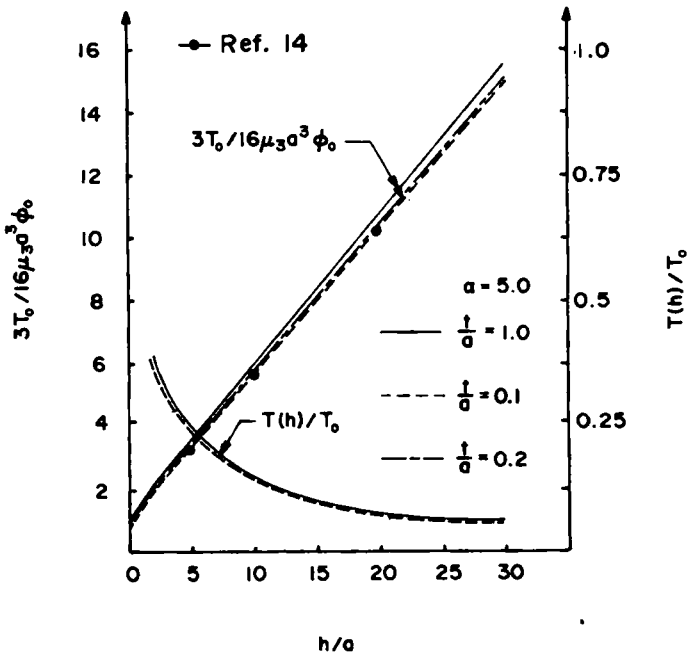

Figure 7. Variation of torsional stiffness and proportion of torque transfer at base for a hollow pier ($\alpha = 5{\cdot}0$)

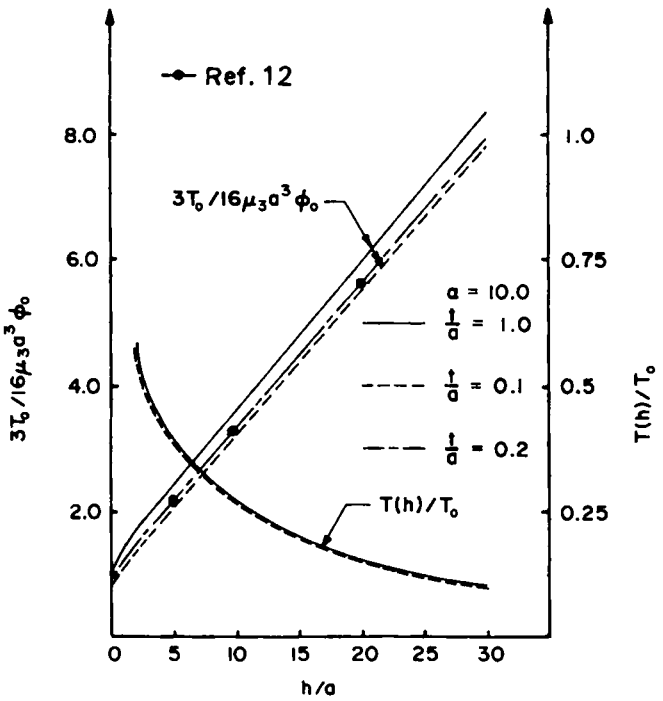

Figure 8. Variation of torsional stiffness and proportion of torque transfer at base for a hollow pier ($\alpha = 10{\cdot}0$)

presented in this paper consider this situation and this special case leads to a convenient parametric representation of the results. Figures 6–8 present the torsional stiffness and the proportion of torque transferred to the base of the rigid pier for a uniform hollow rigid pier, shown in Figure 5(1). Variables include the ratio of the wall thickness to the pier radius (t/a) and the modulus mismatch parameter α. It is evident that the torsional stiffness and the amount of torque transferred at the based are in close agreement with the corresponding values for a solid pier. Except for very short piers ($h/a < 1$) the difference between the torsional stiffness and the base load transfer, respectively, for the hollow and solid piers is always less than ten per cent. Thus for engineering purposes one could accurately model the torsional response of a hollow pier by a solid pier having an identical external diameter. Figures 9–11 present the ratio between the torsional stiffness of a tapered solid pier (Figure 5(b)) and a uniform solid pier of radius a. The proportion of torque transferred at the base is also presented in Figures 9–11 for different values of α and for $\gamma = 0{\cdot}50$, $0{\cdot}75$ and $2{\cdot}0$, respectively. From these Figures it is evident that for a tapered pier the torsional stiffness and the amount of torque transferred at the base differ significantly from these quantities in a uniform solid pier. It is also observed that the ratio T_0/T_u (where T_u is the torsional stiffness of a uniform rigid pier) is practically a constant for a long pier ($h/a > 10$) embedded in a homogeneous half space and, for a layered system, the ratio T_0/T_u approaches a limiting values as h/a increases. The torque transfer curves for a tapered pier having $h/a = 5{\cdot}0$ and $\gamma = 0{\cdot}5$, $0{\cdot}75$, $1{\cdot}0$ and $2{\cdot}0$ are plotted in Figures 12(a) and (b) for $\alpha = 1{\cdot}0$ and $10{\cdot}0$, respectively. It can be seen that for a uniform pier the plot of torque transfer follows practically a linear pattern. A deviation from the linear curve occurs toward the end, due to the existence of stress singularity. For tapered piers, however, the torque transfer plot is not a straight line and takes a convex or a concave form depending on whether the angle β is positive or negative. It is further observed that the torque transfer curve always lies above that corresponding result for a uniform pier if $\gamma > 1$ and lies below it if $\gamma < 1$.

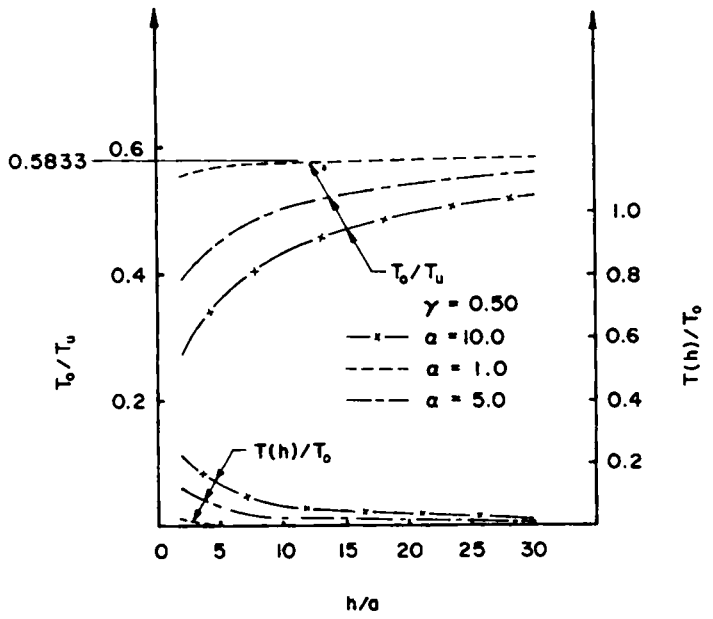

Figure 9. Variation of torsional stiffness and proportion of torque transfer at base for a tapered pier ($\gamma = 0{\cdot}50$)

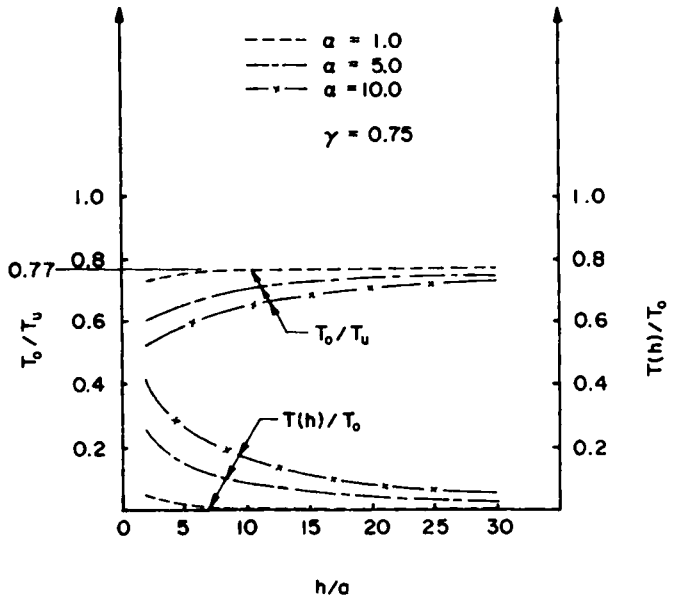

Figure 10. Variation of torsional stiffness and proportion of torque transfer at base for a tatered pier ($\gamma = 0{\cdot}75$)

At this stage attention is focused on a relatively simplified model of the rigid pier problem, with a view to evaluating the torsional stiffness of a tapered pier. We assume that the interface between the layer and half space is smooth; this relaxation of the continuity will yield a lower bound for the torsional stiffness of the pier. The torsional resistance of the pier is obtained by combining the Reissner-Sagoci type torsional restraint which exists at the base and the torque necessary to rotate

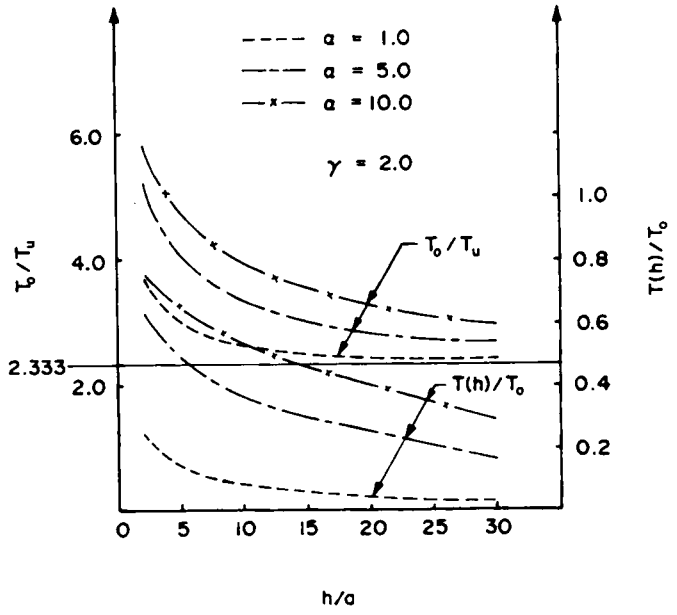

Figure 11. Variation of torsional stiffness and proportion of torque transfer at base for a tapered pier ($\gamma = 2{\cdot}0$)

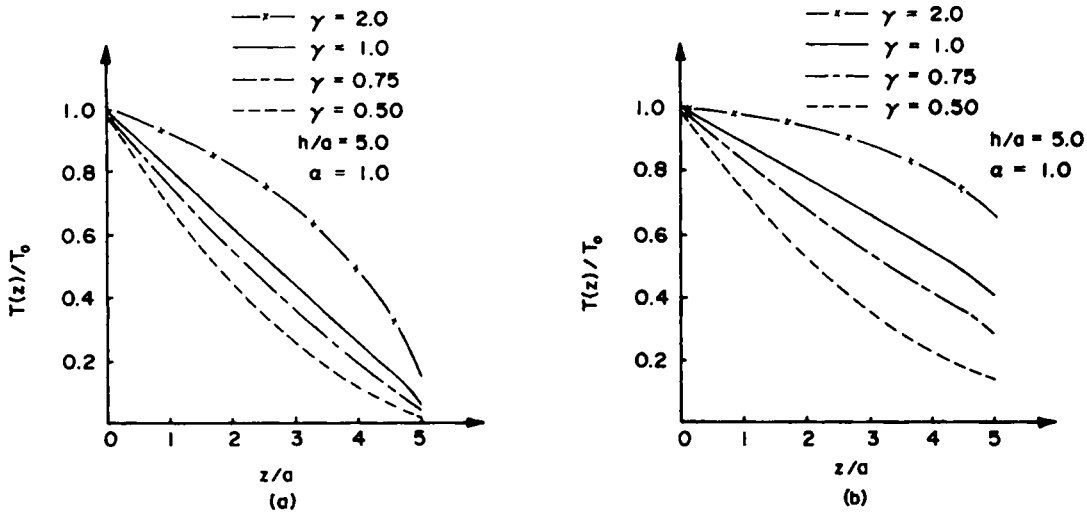

Figure 12. Torque transfer curves for a tapered rigid pier ($h/a = 5{\cdot}0$)

the boundary surface of the top layer by an angle ϕ_0 at any location r described by $r = a + z \tan \beta$, $0 \leqslant z \leqslant h$. In order to estimate the latter quantity we assume that the stress state in the layer is governed by the equation

$$\frac{d\sigma_{r\theta}}{dr} + \frac{2}{r}\sigma_{r\theta} = 0 \tag{19}$$

Then we can evaluate the torque necessary to rotate the surface ($0 \leqslant z \leqslant h$, $r = a + z \tan\beta$,

$0 \leqslant \theta \leqslant 2\pi$) by an angle ϕ_0 as

$$T_1 = 4\pi\mu_1\phi_0[a^2h + ah^2\tan\beta + h^3\tan^2\beta/3]/\cos\beta \tag{20}$$

The sign convention for β is shown in Figure 5. Thus we can express the approximate torque $\bar{T}$ for a tapered bar as

$$\bar{T} = \frac{16\mu_3 a^3\phi_0}{3}\left[\gamma^3 + \frac{3\pi}{4\alpha\cos\beta}\left(\frac{h}{a} + \frac{h^2}{a^2}\tan\beta + \frac{h^3}{a^3}\tan^2\beta/3\right)\right] \tag{21}$$

or by considering the geometry of the pier we have

$$\bar{T} = \frac{16\mu_3 a^3\phi_0}{3}\left[\gamma^3 + \frac{\pi h}{4\alpha a\cos\beta}(\gamma^2 + \gamma + 1)\right] \tag{22}$$

when $\beta = 0$ (i.e. for a uniform bar)

$$\bar{T}_u = \frac{16\mu_3 a^3\phi_0}{3}\left[1 + \frac{3\pi h}{4\alpha a}\right] \tag{23}$$

which is equivalent to the approximate result given by Luco[2] and Randolph.[12] If we examine a very long bar where $(h/a) \gg \gamma^3$ then

$$\frac{\bar{T}}{\bar{T}_u} = (\gamma^2 + \gamma + 1)/3 \tag{24}$$

Table I presents a comparison of values of torsional stiffness computed by using equation (21) and the actual values computed from the proposed discretization scheme. The approximate and analytical values for the stiffness presented in Table I agree very closely. Thus for practical purposes one could obtain an engineering estimation of torsional stiffness using equation (21). However, for short bars ($h/a \leqslant 2$) with considerable slope, significant differences (especially for large α) exist between the two values, primarily due to the existence of a three-dimensional stress state in the layer. Such cases are however quite rare in geotechnical engineering applications. Furthermore for hollow piers we could use equation (23) to obtain a reasonably accurate estimation of stiffness. According to equation (24) for a long pier ($\bar{T}/\bar{T}_u$) approaches the limit $(\gamma^2 + \gamma + 1)/3$ as h/a increases. Thus the ratio ($\bar{T}_o/\bar{T}_u$) plotted in Figures 9–11 should follow a similar behaviour for large values of (h/a) since the approximate formulae provide good accuracy in this range. The curves presented in Figures 9–11 clearly show the transition towards a limiting value which is close to $(\gamma^3 + \gamma + 1)/3$.

Next, we consider the torque–twist relationship developed by Selvadurai[13,14] for a rigid hemispheroidal inclusion (Figure 13) embedded in an isotropic homogeneous elastic medium. It is

Table I. Comparison of torsional stiffness values obtained by analytical method and approximate formula; $\gamma = 0{\cdot}5$

h/a	$\alpha = 1{\cdot}0$		$\alpha = 10{\cdot}0$	
	$3T_0/16\mu_3a^3\phi_0$	$3\bar{T}/16\mu_3a^3\phi_0$	$3T_0/16\mu_3a^3\phi_0$	$3\bar{T}/16\mu_3a^3\phi_0$
2·0	3·41	2·95	0·48	0·41
5·0	7·43	7·03	0·87	0·81
10·0	14·43	13·88	1·57	1·50
15·0	21·48	20·75	2·26	2·19
20·0	28·40	27·61	2·94	2·87
30·0	42·91	41·35	4·39	4·25

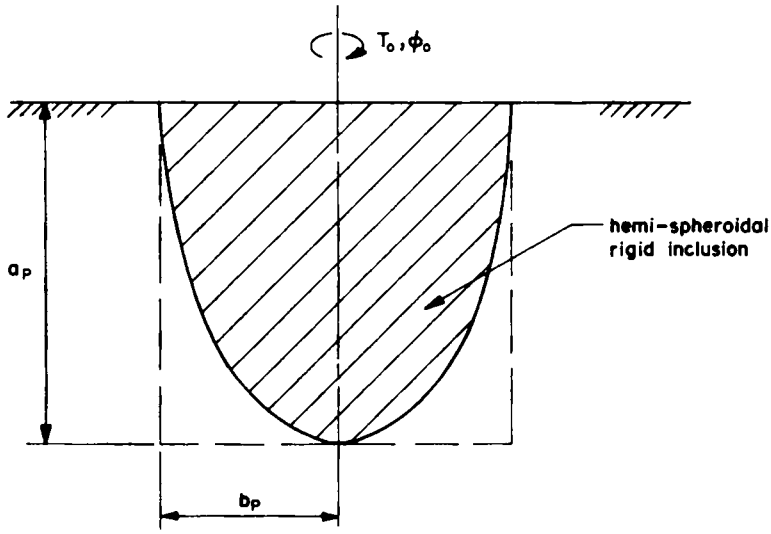

Figure 13. Geometry of hemi-spheroidal rigid inclusion

found that the torque–twist relationship can be expressed as

$$\frac{3T_o}{16\mu_1 a^3 \phi_0} = c(\lambda) F(\lambda) \tag{25}$$

where

$$F(\lambda) = \frac{\pi(1-\lambda^2)^{3/2}}{\lambda\left[2(1-\lambda^2)^{1/2} - \lambda^2 \ln\left\{\frac{1+(1-\lambda^2)^{1/2}}{1-(1-\lambda^2)^{1/2}}\right\}\right]}$$

and

$$\lambda = \frac{b_p}{a_p}$$

In order to estimate the torsional stiffness of a tapered rigid pier we set $\lambda = a/h$ and equate the surface areas of the tapered pier and the hemispheroidal inclusion. In doing so, the function $c(\lambda)$ is

Table II. Comparison of numerical values of $3T_0/16\mu_3 a^3\phi_0$ for a tapered rigid pier embedded in a homogeneous half space ($\alpha = 1$)

h/a	$\gamma = 0{\cdot}75$			$\gamma = 0{\cdot}50$		
	Analytical	Spheroidal approximation: equation (25)	Plane approximation: equation (21)	Analytical	Spheroidal approximation: equation (25)	Plane approximation: equation (21)
2	4·47	4·91	4·08	3·41	3·94	2·95
5	9·91	10·34	9·51	7·43	8·21	7·03
10	19·01	19·48	18·58	14·43	15·46	13·88
15	28·21	28·67	27·66	21·48	22·75	20·75
20	37·44	37·87	36·74	28·40	30·05	27·61
30	56·52	56·30	54·91	42·91	44·67	41·35

found to be

$$c(\lambda) = \left\{ \frac{2\gamma \sec\beta (1-\lambda^2)^{1/2}}{[\lambda(1-\lambda^2)^{1/2} + \sin^{-1}(1-\lambda^2)^{1/2}]} \right\}^{3/2} \tag{26}$$

Table II presents the comparison of numerical values of torsional stiffness obtained from the discretized analytical scheme, the spheroidal approximation given by equation (25) and the plane approximation given by equation (21). It is clear from the results presented in Table II that the approximate stiffness value computed by equation (25) provides an accurate estimation for long piers ($h/a \geqslant 10$). Unlike the plane approximation considered earlier the spheroidal approximation cannot be applied in cases where $\gamma > 1$ or $\alpha \neq 1{\cdot}0$.

The present solution scheme does not estimate the order of stress singularity at the base of the bar; however, the numerical values of T_j confirm the existence of singular behaviour of stresses at the base. As far as global results, such as torque–twist relationships, are concerned the effects of such singularities are negligible.[3] In cases where it is necessary to estimate the order of stress singularity one could apply William's method as exemplified in Reference 3 to obtain an accurate estimation of the order of singularity.

ACKNOWLEDGEMENTS

The work described in this paper was supported by a Natural Sciences and Engineering Research Council of Canada Grant No. A3866, awarded to one of the authors (APSS).

REFERENCES

1. H. G. Poulos, 'Torsional response of piles', *J. Geotech. Eng. Div. ASCE*, **101**, (GT10), 1019–1035 (1975).
2. J. E. Luco, 'Torsion of a rigid cylinder embedded in an elastic half space', *J. Appl. Mech. ASME*, **43**, 419–423 (1976).
3. P. Karasudhi, R. K. N. D. Rajapakse and B. Y. Hwang, 'Torsion of a long cylindrical elastic bar partially embedded in a layered elastic half space', *Int. J. Solids Struct.*, **20**, 1–11 (1984).
4. R. Muki and E. Sternberg, 'Elastostatic load transfer to a half space from a partially embedded axially loaded rod', *Int. J. Solids Struct.*, **6**, 69–90 (1970).
5. R. Muki, 'Asymmetric problems of the theory of elasticity for a semi-infinite solid and a thick plate', in I. N. Sneddon and R. Hill (eds) *Progress in Solid Mechanics* 1, North Holland, Amsterdam, Interscience, New York, (1960), pp. 399–439.
6. I. N. Sneddon, *Fourier Transforms*, McGraw-Hill, New York, 1951.
7. K. S. Chan, P. Karasudhi and S. L. Lee, 'Force at a point in the interior of a layered elastic half space', *Int. J. Solids Struct.*, **10**, 1179–1199 (1974).
8. G. N. Watson, *A Treatise on the Theory of Bessel Functions*, Cambridge University Press, 1944.
9. G. Eason, B. Noble and I. N. Sneddon, 'On certain integrals of Lipschitz–Hankel type involving products of Bessel functions', *Phil. Trans. R. Soc. London A*, **247**, 529–551 (1955).
10. C. Heuman, 'Tables of complete elliptic integrals', *J. Math. Phys.* **20**, 127–206 (1941).
11. M. Abramowitz and I. A. Stegun, *Handbook of Mathematical Functions*, Dover, New York, 1972.
12. M. F. Randolph, 'Piles subjected to torsion', *J. Geotech., Eng. Div. ASCE*, **107**, (GT8), 1095–1111 (1981).
13. A. P. S. Selvadurai, 'On the estimation of the deformability characteristics of an isotropic elastic soil medium by means of a vane test', *Int. j. numer. anal. methods geomech.*, **3**, 231–243 (1979).
14. A. P. S. Selvadurai, 'Torsional stiffnesses of rigid piers embedded in isotropic elastic soils', in J. A. Langer, E. Mosely and C. Thompson (eds), *Laterally Loaded Deep Foundations; Analysis and Performance*, ASTM STP 835, pp. 49–55.